Electronic Supplementary Material (ESI) for Materials Advances.

Supporting Information

Enhancing Catalytic Activity of CdX and ZnX (X = S, Se and Te) Nanostructures for Hydrogen Evolution Reaction via Transition Metal Doping

Feifei Xia,‡* Li Shu,‡ Yingpin Wen,‡ Fengli Yang,‡ and Chunzhi Zheng‡

‡*School of Chemical and Environmental Engineering, Jiangsu University of Technology, Changzhou 213001, Jiangsu, P. R. China*

E-mail: ffxia@jsut.edu.cn

Table S1 The calculated bandgaps of pristine CdX and ZnX (X = S, Se and Te) in bulk phase at GGA-PBE and HSE06 level in comparison with experimental data[1-3]

Methods	CdS	CdSe	CdTe	ZnS	ZnSe	ZnTe
GGA-PBE	1.15	0.63	0.57	2.16	1.36	1.11
HSE06	2.41	1.86	1.47	3.56	2.55	2.39
Expt[1-3]	**2.485**	**1.75**	**1.43**	**3.68**	**2.7**	**2.26**

Table S2. Free energies for the intermediates (*H) absorption on the pristine and TM doped CdX and ZnX (X = S, Se and Te) surface.

System	CdS		CdSe		CdTe		ZnS		ZnSe		ZnTe	
	ΔG_{*H}/eV		ΔG_{*H}/eV		ΔG_{*H}/eV		ΔG_{*H}/eV		ΔG_{*H}/eV		ΔG_{*H}/eV	
	H-M	H-X	H-M	H-X	H-M	H-X	H-M	H-X	H-M	H-X	H-M	H-X
pristine	2.00	1.07	1.93	1.12	1.73	1.45	1.95	1.64	1.80	1.64	1.52	1.78
Fe	0.84	0.79	0.77	0.86	0.56	0.88	0.57	1.13	0.54	0.98	0.25	0.65
Co	0.35	0.44	0.43	0.50	0.34	0.65	0.34	0.83	0.33	0.59	0.25	0.64
Ni	0.32	**-0.03**	0.30	**0.19**	0.20	0.37	**0.28**	0.53	0.24	0.34	**0.09**	0.45
Cu	-0.48	-0.28	**-0.10**	-0.22	**0.17**	**0.08**	-0.45	**0.01**	**0.17**	**-0.06**	0.36	**0.25**
Pd	0.29	0.10	0.19	0.31	**0.06**	0.27	**-0.06**	0.25	**0.05**	0.19	0.17	0.52
Pt	0.38	0.30	**0.06**	0.50	-0.12	0.42	-0.001	0.77	-0.18	0.34	**0.01**	0.66

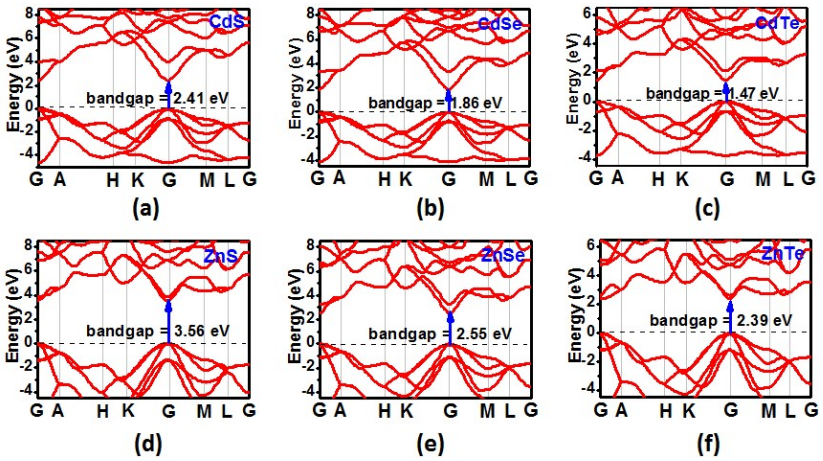

Figure S1. Calculated band structures of pristine (a) CdS, (b) CdSe, (c) CdTe, (d) ZnS, (e) ZnSe and (f) ZnTe in bulk phase using HSE06 methods. The dashed black line is the Fermi level.

As shown in Figure S1, the general features of the band structures of pristine CdX and ZnX (X = S, Se, Te) are similar with differences in bandwidths and all these compound materials are direct bandgaps. The valence bandwidth of CdX is smaller than that of ZnX, which probably arises from the hybridization accompanying the change in bonding from more ionic to more covalent, as Zn is replaced by Cd. In addition, the bandwidth of CdX and ZnX increases as S is replaced by Se and Se by Te in hexagonal phases. In all cases, the valence band maximum and the conduction band minimum occur at the G point, hence these compounds are semiconductors with direct energy band gaps. For the same X atom, this direct energy bandgap decreases from Zn to Cd.

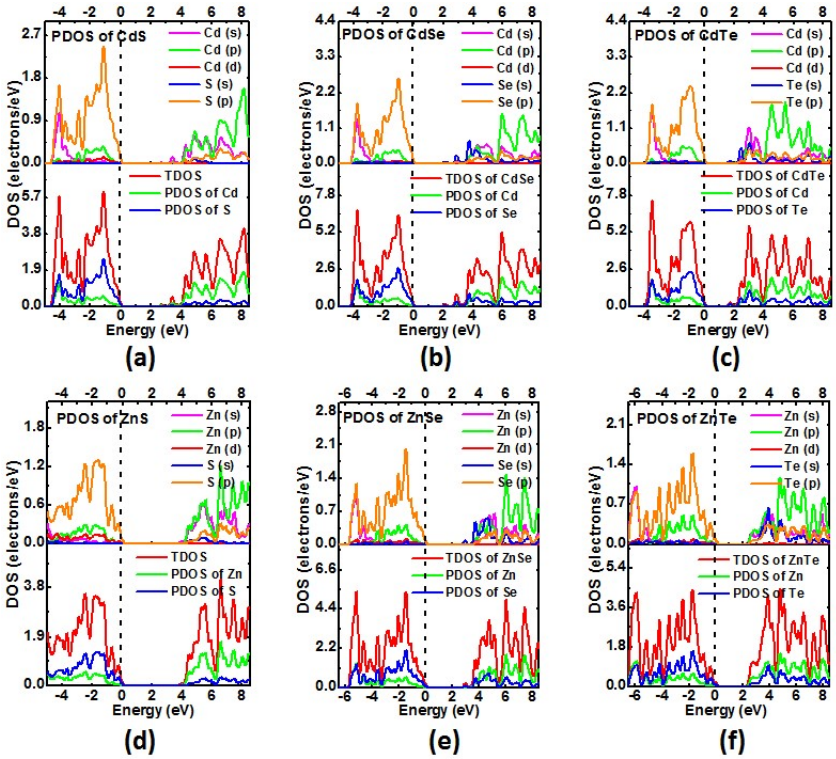

Figure S2. Calculated TDOS and PDOS of Cd/Zn and X atoms in CdX and ZnX for pristine (a) CdS, (b) CdSe, (c) CdTe, (d) ZnS, (e) ZnSe and (f) ZnTe in bulk phase using HSE06 methods. The dashed black line is the Fermi level.

To understand the bonding characteristics of pristine CdX and ZnX (X = S, Se, Te), We calculated their the total density of state (TDOS) and PDOS with HSE06 method, and the results are depicted in Figure S2. It can be noted that the electron density of state (DOS) is similar for all pristine CdX and ZnX (X = S, Se, Te), with some small differences in details. The major contribution to the occupied part of the electron DOS around the Fermi energy comes from the p orbitals of the X atom and the s orbitals of Zn and Cd. The corresponding PDOS of CdX and ZnX in Figure S2 illustrates that the valence band of CdX and ZnX is dominated by Cd/Zn 4p, S 4p, Se 5p and Te 6p states, indicating hybridization between those orbitals and a covalent bond character.

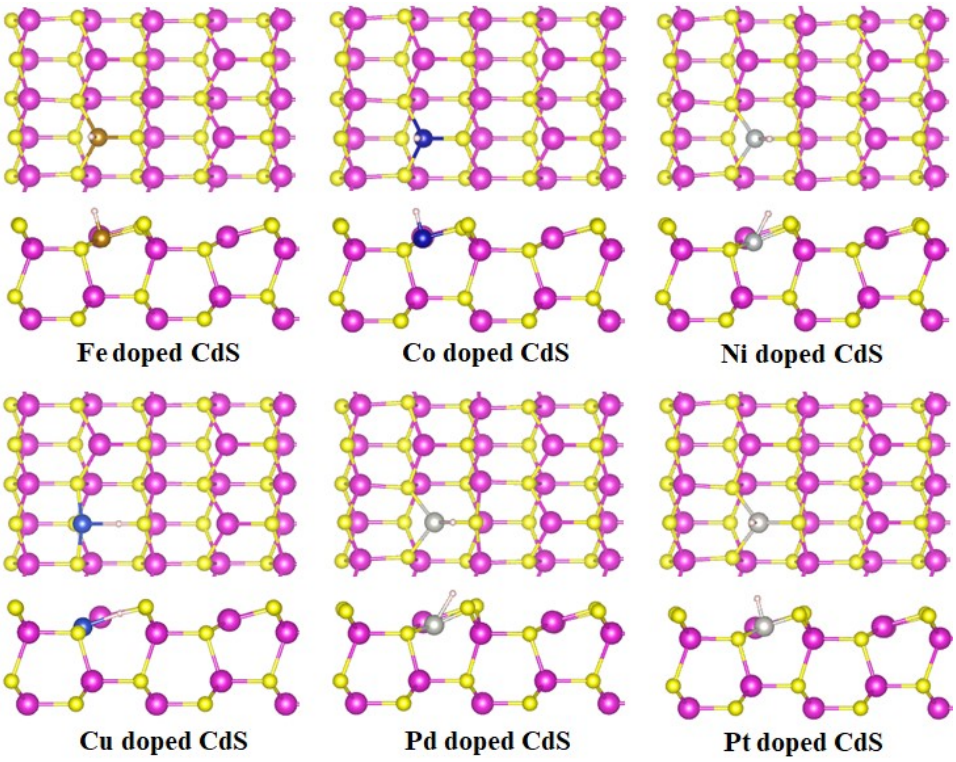

Figure S3. The optimized structures of hydrogen adsorption on TM doped CdS surface at transition metal active site.

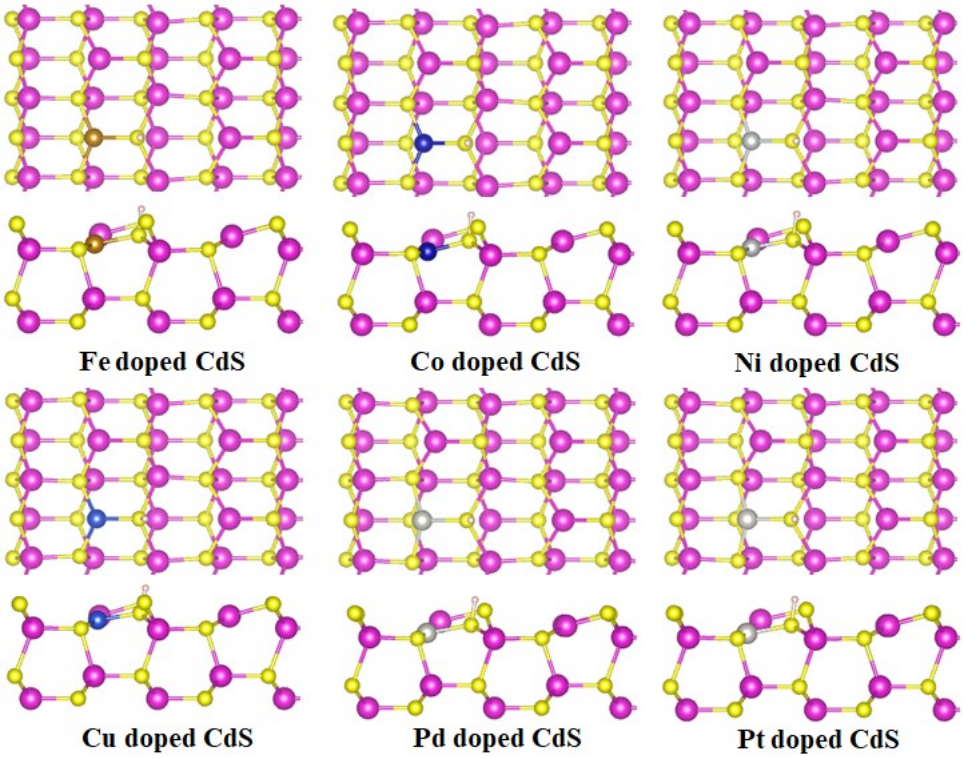

Figure S4. The optimized structures of hydrogen adsorption on TM doped CdS surface at S active site.

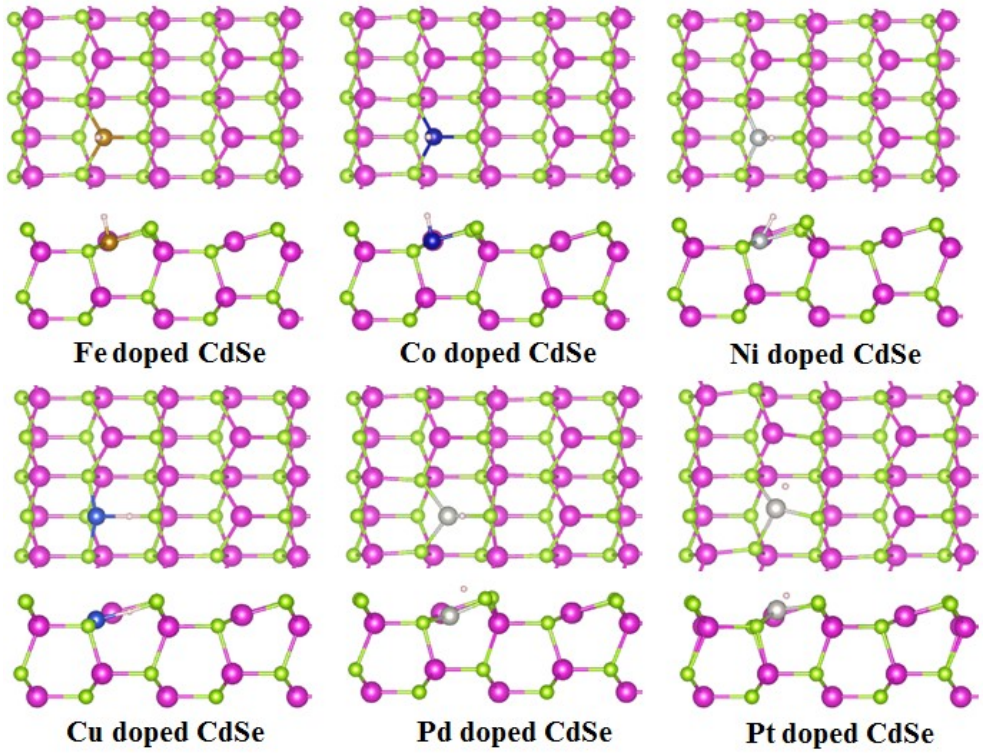

Figure S5. The optimized structures of hydrogen adsorption on TM doped CdSe surface at transition metal active site.

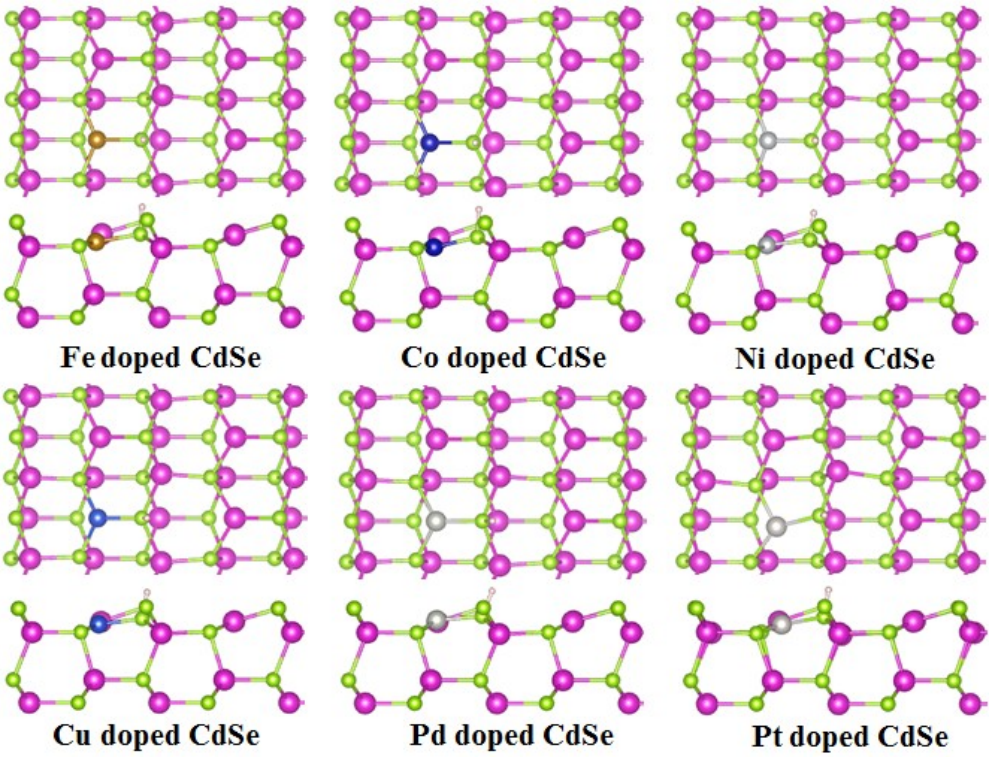

Figure S6. The optimized structures of hydrogen adsorption on TM doped CdSe surface at Se active site.

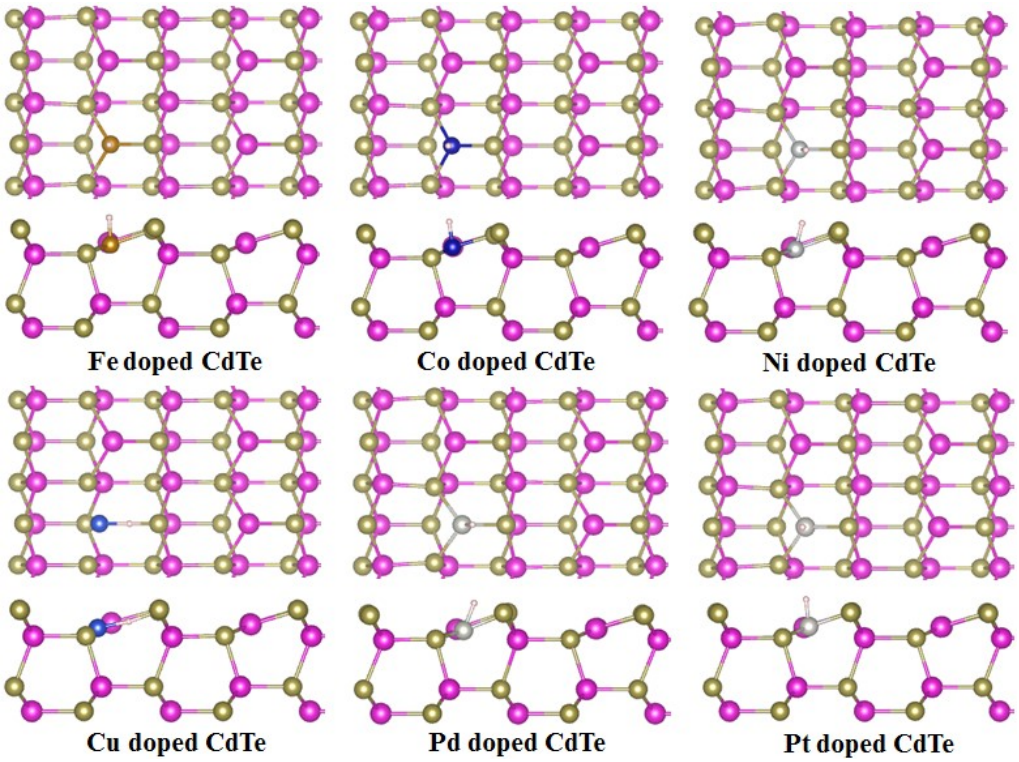

Figure S7. The optimized structures of hydrogen adsorption on TM doped CdTe surface at transition metal active site.

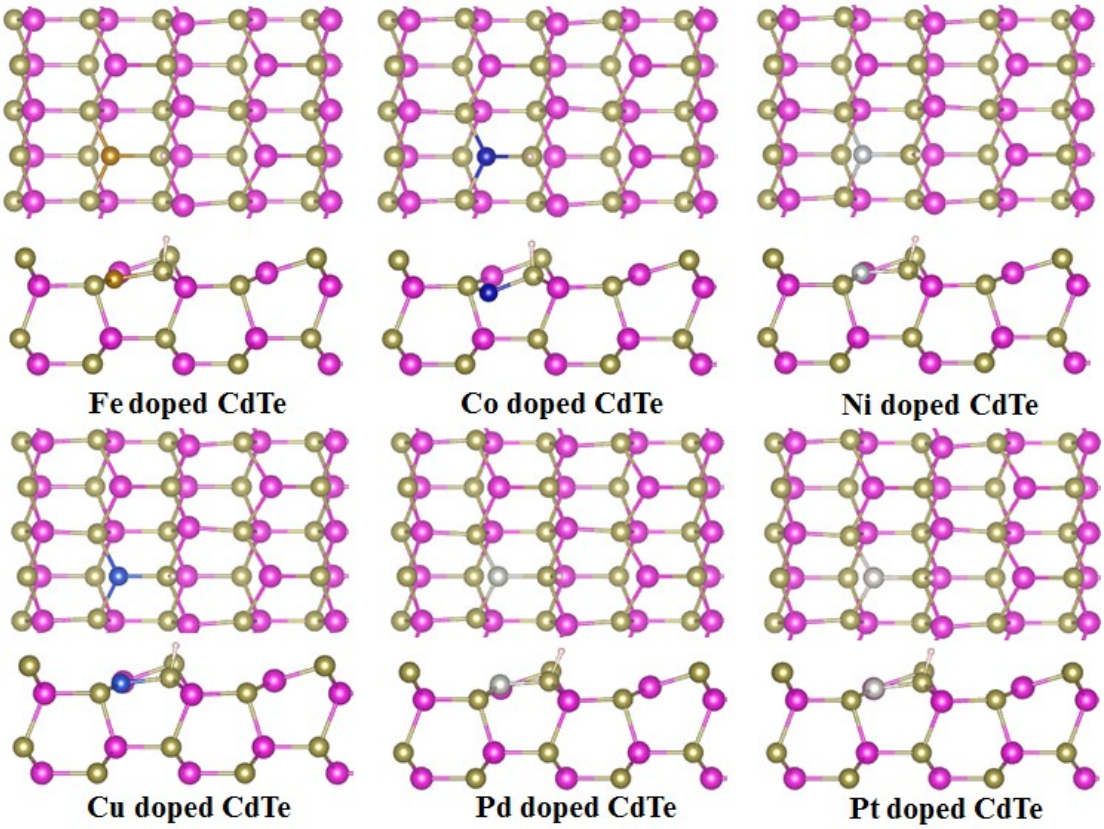

Figure S8. The optimized structures of hydrogen adsorption on TM doped CdSe surface at Te active site.

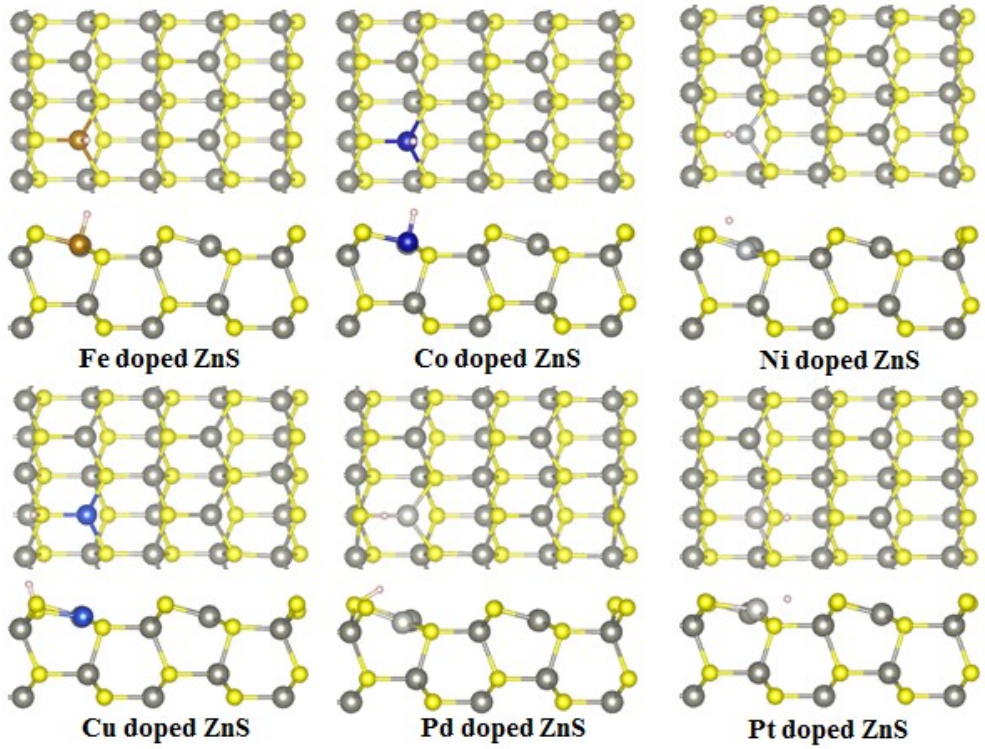

Figure S9. The optimized structures of hydrogen adsorption on TM doped ZnS surface at transition metal active site.

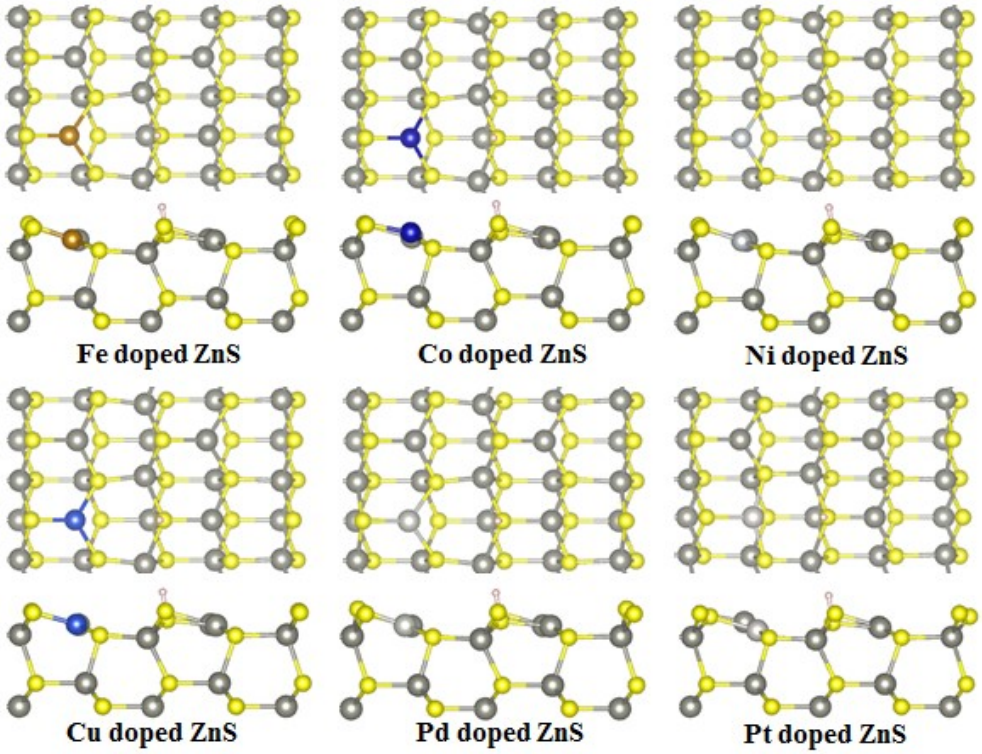

Figure S10. The optimized structures of hydrogen adsorption on TM doped ZnS surface at S active site.

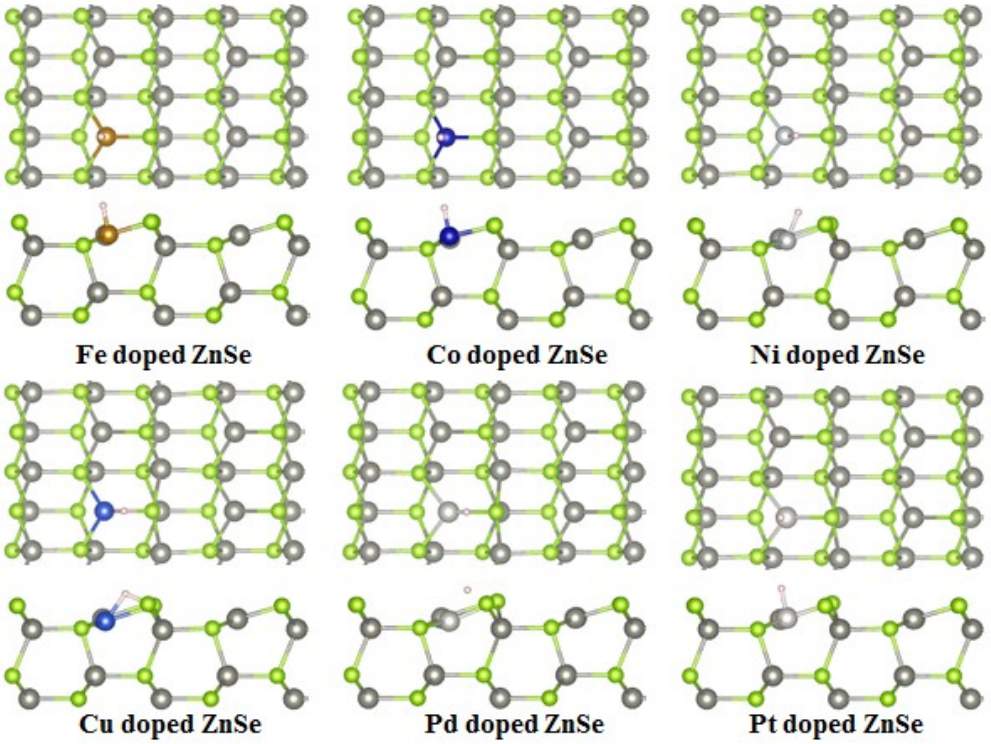

Figure S11. The optimized structures of hydrogen adsorption on TM doped ZnSe surface at transition metal active site.

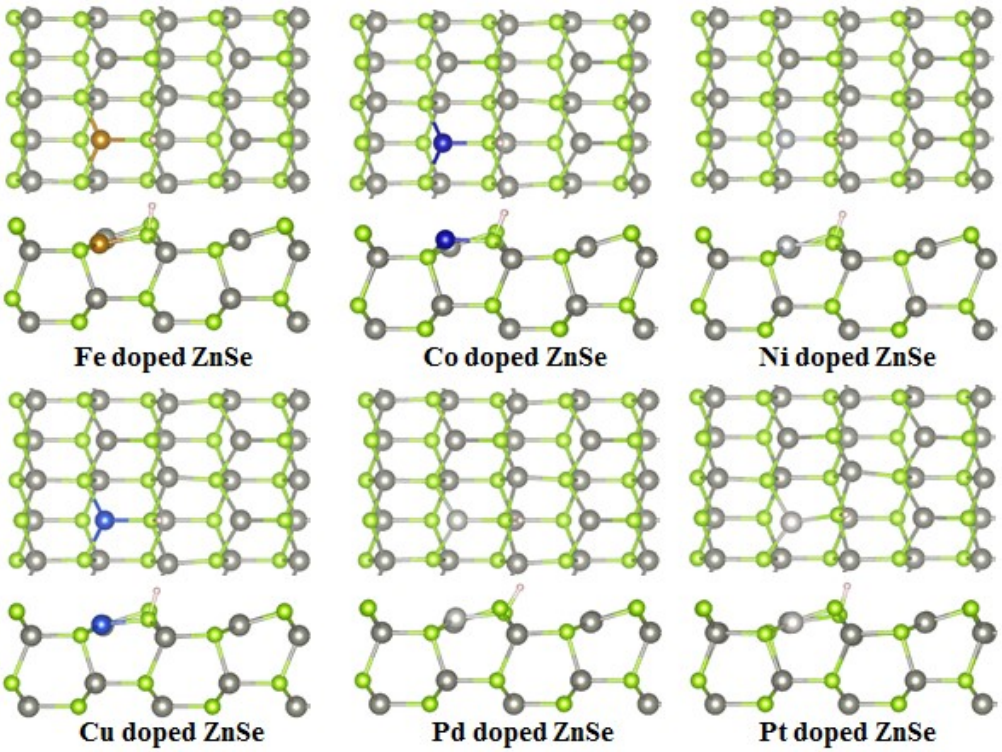

Figure S12. The optimized structures of hydrogen adsorption on TM doped ZnSe surface at Se active site.

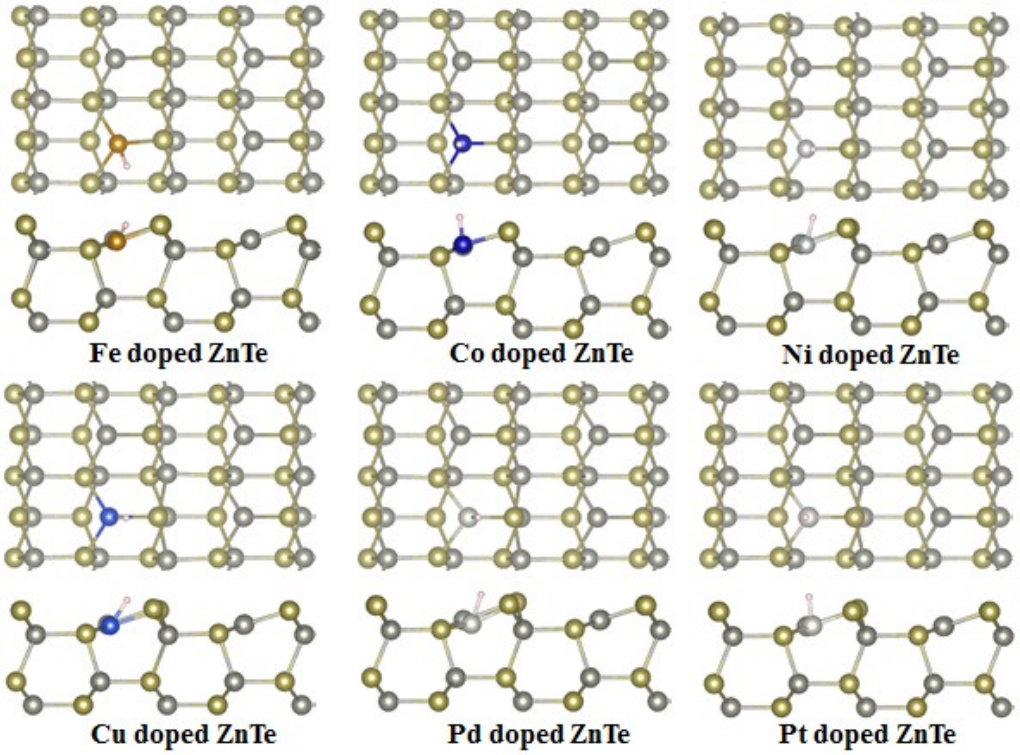

Figure S13. The optimized structures of hydrogen adsorption on TM doped ZnTe surface at transition metal active site.

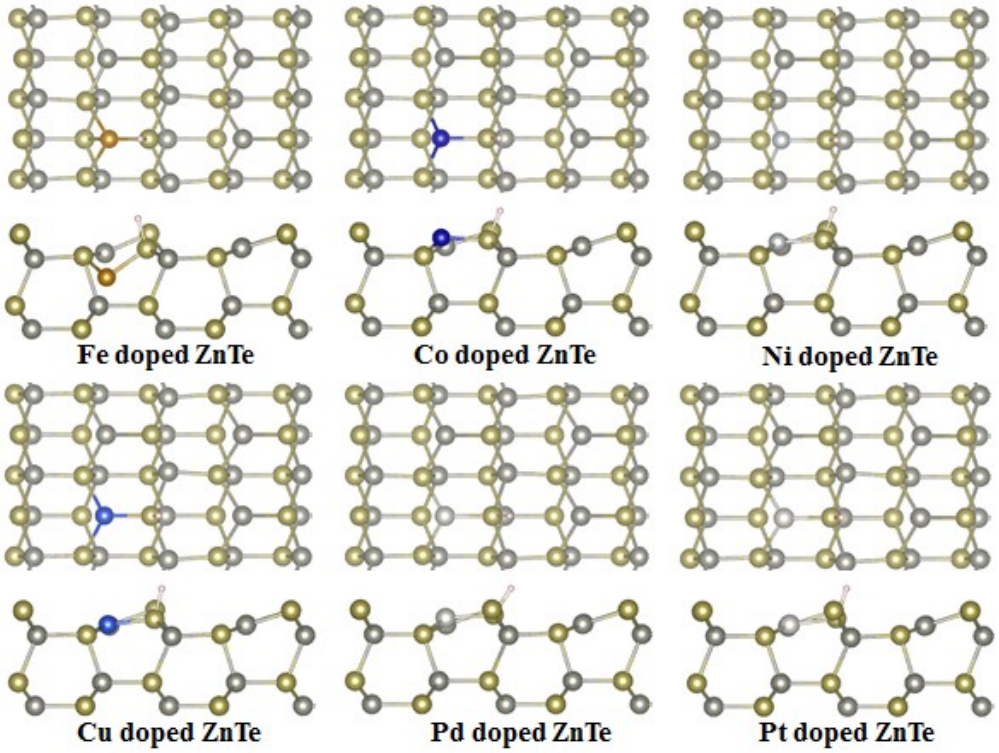

Figure S14. The optimized structures of hydrogen adsorption on TM doped ZnTe surface at Te active site.

REFERENCES

[1] Guido Petretto, Shyam Dwaraknath, Henrique P. C. Miranda, Donald Winston, Matteo Giantomassi, Michiel J. van Setten, Xavier Gonze, Kristin A. Persson, Geoffroy Hautier, Gian-Marco Rignanese, High-throughput density functional perturbation theory phonons for inorganic materials, *Scientific Data*, **2018**, *5*,180065

[2] Aminoff, G. Untersuchungen ueber die kristallstrukturen von wurtzit und rotnickelkies. *Zeitschrift fur Kristallographie*, **1923**, *58*, 203-219;

[3] Wyckoff, R. W. G. Second edition. Interscience Publishers, New York, New York Note: wurtzite structure. *Crystal Structures*, **1963**, *1*, 85-237